Title: Structural evolution and *microwave dielectric properties in $Sr_2(Ti_{1-x}Sn_x)O_4$ ceramics

Authors: Bing Liu, Yu Hui Huang, Kai Xin Song, Lei Li, Xiang Ming Chen

PII: S0955-2219(18)30241-3
DOI: https://doi.org/10.1016/j.jeurceramsoc.2018.04.029
Reference: JECS 11839

To appear in: *Journal of the European Ceramic Society*

Received date: 6-2-2018
Revised date: 11-4-2018
Accepted date: 13-4-2018

Please cite this article as: Liu B, Huang YH, Song KX, Li L, Chen XM, Structural evolution and *microwave dielectric properties in $Sr_2(Ti_{1-x}Sn_x)O_4$ ceramics, *Journal of the European Ceramic Society* (2010), https://doi.org/10.1016/j.jeurceramsoc.2018.04.029

Structural evolution and microwave dielectric properties in $Sr_2(Ti_{1-x}Sn_x)O_4$ ceramics

Bing Liu[a,b,§,*], Yu Hui Huang[b,§], Kai Xin Song[a], Lei Li[b], and Xiang Ming Chen[b,*]

a. *College of Electronic Information and Engineering, Hangzhou Dianzi University, Hangzhou 310018, China.*

b. *Laboratory of Dielectric Materials, School of Materials Science and Engineering, Zhejiang University, Hangzhou 310027, China.*

§ The authors contributed equally to this work and should be listed as co-first authors.

*Corresponding authors. E-mail: liubing@hdu.edu.cn, xmchen59@zju.edu.cn

Abstract

The structure and microwave dielectric properties of $Sr_2(Ti_{1-x}Sn_x)O_4$ ceramics were determined in the entire composition range of x = 0–1.0. X-ray diffraction patterns and Raman spectra indicated a composition-induced onset of octahedral tilting at x = 0.75, and the crystal structure transformed from tetragonal (*I*4/*mmm*) to orthorhombic (*Pccn*). An obvious change of grain morphology was observed in the phase transformation region as well. The variations of the microwave dielectric properties with composition were systematically investigated and the effect of octahedral tilting on the evolution of τ_f value was emphasized. Moreover, the relationship between τ_ε and tolerance factor of the present ceramics was revealed and compared with the empirical rule in perovskite structure. The role of tolerance factor in designing the materials with required performance was highlighted.

Keywords: $Sr_2(Ti_{1-x}Sn_x)O_4$ ceramics, octahedral tilting, microwave dielectric properties

§ The authors contributed equally to this work and should be listed as co-first authors.

*Corresponding authors. E-mail: liubing@hdu.edu.cn, xmchen59@zju.edu.cn

1. Introduction

Over decade, with the rapid development of wireless communication technology, microwave dielectric ceramics have received wide attentions as the key materials for microwave resonators, filters and other passive devices [1,2]. Moreover, the recent progress in Internet of Things (IoT), intelligent transport systems (ITS), etc. has resulted in an increasing need for new designs of microwave dielectric components and demands materials with suitable dielectric constant (ε_r), low dielectric loss (high quality factor Q = 1/tanδ) and near-zero temperature coefficient of resonant frequency (τ_f) [3].

Up to now, large amounts of studies have been carried out on the development of microwave dielectric ceramics with Ruddlesden-Popper structure [4-6]. Among these, great progress has been achieved in the $Sr_{n+1}Ti_nO_{3n+1}$ (n = 1, 2) system. Lee *et al*. found out that the $Sr_{n+1}Ti_nO_{3n+1}$ films exhibited fascinating physico-chemical properties and exceptionally low dielectric loss at microwave frequency [7]. From the perspective of bulk ceramics, our previous study has systematically investigated the synthesis of Sr_2TiO_4 ceramics and outstanding microwave dielectric properties (ε_r = 42, Qf = 145,000 GHz, τ_f = 130 ppm/^{o}C) were also obtained [8]. Compared with the typical low-loss candidates such as $Ba(Mg_{1/3}Ta_{2/3})O_3$ and $Ba(Zn_{1/3}Ta_{2/3})O_3$ (ε_r = 25~30, Qf = 150,000 ~ 250,000 GHz, τ_f ~ 0 ppm/^{o}C) [9,10], Sr_2TiO_4 without noble elements has the merits of easy preparation and low cost. However, the large τ_f has greatly limited its practical applications and should be further optimized.

Based on the previous work by Reaney *et al.*, it has been widely accepted that the octahedral tilting transition is a major factor in controlling the τ_f [11,12]. Moreover, the recent work by Wang *et al.* has successfully revealed the octahedral tilting mechanism in the Ruddlesden-Popper structure and the effect of smaller tolerance factor (t) in inducing octahedral tilting was highlighted [13]. In $(Sr_{1-x}Ca_x)_3Ti_2O_7$ solid solution system, Wise *et al.* reported a significant reduction of τ_f value from 359 ppm/^{o}C to 50 ppm/^{o}C when the structure transformed from tetragonal to orthorhombic (t decreases from 0.971 to 0.938) [14]. For $(Sr_{1-x}Ca_x)_2TiO_4$ ceramics, as the end-member "Ca_2TiO_4" does not exist under normal condition, the solid solubility of Ca^{2+} in A-site is limited.

More effective modifications of octahedral tilting should be expected through B-site substitutions. As the radius of Sn^{4+} (0.69 Å) is larger than Ti^{4+} (0.609 Å), the substitution of Sn^{4+} for Ti^{4+} could lead to the onset of octahedral tilting and optimize the microwave dielectric properties subsequently. Moreover, the end-member Sr_2SnO_4 has been prepared by Fu *et al.* and the space group was confirmed to be *Pccn* with $a^-b^0c^0$ rotation [15]. Motivated by this, the correlation between the onset of octahedral tilting and microwave dielectric properties in $Sr_2(Ti_{1-x}Sn_x)O_4$ ceramics is worth studying and may trigger a new breakthrough in the application of high performance microwave dielectric ceramics.

In the present work, $Sr_2(Ti_{1-x}Sn_x)O_4$ (x = 0, 0.25, 0.50, 0.75, 0.80, 1.0) ceramics are prepared using a standard solid-state reaction method. The effects of Sn^{4+} substitution for Ti^{4+} on the evolution of crystal structure are systematically investigated. Meanwhile, the relationships between crystal structure and microwave dielectric properties (especially the τ_f value) are emphasized.

2. Experimental procedure

$Sr_2(Ti_{1-x}Sn_x)O_4$ ceramics were prepared using high purity $SrCO_3$ (99.95%), TiO_2 (99.99%) and SnO_2 (99.99%) oxide powders as raw materials. The stoichiometric raw powders were weighed and ball milled in ethanol media for 24h. After drying, the powders were calcined at 1150ºC~1250ºC in air for 3h, then re-milled and mixed with 4 wt% PVA (polyvinyl alcohol) solution. The homogeneous powders were pressed into pellets of 12 mm in diameter and 6 mm in height, and sintered at 1500ºC–1700ºC in air for 3h to obtain the dense ceramics.

Microstructures of the polished and thermal etched samples were observed by scanning electron microscopy (SEM) (S-3400, Hitachi, Tokyo, Japan). The thermal etching was conducted at a temperature 50 ºC lower than the sintering temperature for 30 min. Room temperature powder X-ray diffraction (XRD) with Cu$K\alpha$ (λ = 1.5406 Å) radiation (D/max 2550/PC, Rigaku Co., Tokyo, Japan) was utilized to analyze the phase compositions. Rietveld refinement was employed to further understand the evolution of crystal structure. Room temperature Raman spectra were carried out using an HR-

800 LabRaman (Jobin Yvon, Longjumeau, France) equipped with a Peltier-cooled charge-coupled device and an integral Raman microscope. Ar^+ ion laser (λ = 514.532 nm) with an output of 20 mW was used as the excitation source. The spectra was recorded from 50 to 1000 cm^{-1} and the spectra resolution was about 1 cm^{-1}.

The microwave dielectric properties were evaluated using a vector network analyzer (E8363B, Agilent Technologies Inc., Santa Clara, CA). *Qf* value was measured using the resonant-cavity method [16], while ε_r and τ_f were measured using the parallel plate method [17]. The measurement of τ_f was carried out from 20 ~ 80ºC and was calculated using the following formula:

$$\tau_f = \frac{f_{80} - f_{20}}{f_{20} \times (80 - 20)} \times 10^6 \ \text{(ppm/°C)} \quad (1)$$

where, f_{20} and f_{80} denoted the resonant frequencies at 20°C and 80°C, respectively.

3. Results and discussion

Fig. 1(a) shows the normalized XRD patterns of $Sr_2(Ti_{1-x}Sn_x)O_4$ ceramics obtained at their optimal sintering temperatures. All the diffraction patterns can be assigned to those for Sr_2TiO_4 (JCPDS card #39-1471) and Sr_2SnO_4 (JCPDS card #10-4447). No obvious peaks corresponding to secondary phases are observed, which confirms the formation of $Sr_2(Ti_{1-x}Sn_x)O_4$ solid solutions in the whole composition range. On the other hand, the present ceramics undergo an apparent structural evolution from tetragonal (*I*4/*mmm*) to orthorhombic (*Pccn*) with increasing *x*. To further reveal the structural transformation, Fig. 1(b) shows the enlarged diffraction patterns in the 2θ range of 41.5º~44.5º. The diffraction patterns of $x \geq 0.75$ could be well indexed to the patterns of Sr_2SnO_4. Besides, it is worth noting that the corresponding diffraction peaks shifts to lower 2θ angle in the composition range of $0 < x < 0.75$ and remains relatively stable with further increasing *x*. The peak shift when $x < 0.75$ is mainly due to the larger ion substitution of Sn^{4+} for Ti^{4+}. While, the following change should mainly ascribe to the relatively stable lattice parameters evolution in *Pccn* space group, which was reported by Fu *et al.* [15]. Therefore, it is inferred that the structural transformation occurs at around $x = 0.75$ and turns to orthorhombic thereafter.

To further investigate the crystal structure and phase compositions, Rietveld refinement is carried out using Fullprof software. The crystal structures of Sr_2TiO_4 and Sr_2SnO_4 are adopted as the initial structure models and the ion occupancy is revised according to the nominal composition before the refinement. Fig. 2 shows the calculated and observed diffraction profiles of x = 0.75 and 1.0 compositions. The refined structural parameters, phase compositions and reliability factors are listed in Table 1. The calculated diffraction profiles are in good agreement with the observed ones, as confirmed by the low amplitudes of the difference lines (see blue lines in Fig. 2). In addition, the good reliability factors of the refinement (R_p, R_{wp} and χ^2) indicate that the structure models are valid and the refinement results are reliable. As seen in Table 1, the weight percentage of the orthorhombic phase at x = 0.75 is 34.42% and the x = 1.0 composition indicates a pure orthorhombic structure, which further confirms the above-mentioned structural evolution process. Besides, the inset figures in Fig. 2 give detailed fitting profiles, where the structure differences are further confirmed.

Moreover, Raman spectra of the present ceramics are measured as it is very sensitive to the structure and could be applied as a powerful tool in correlating vibrational characteristics to microwave dielectric properties [18,19]. As shown in Fig. 3, the Raman spectra of Sr_2TiO_4 shows four first order Raman modes at 122 cm^{-1}, 204 cm^{-1}, 284 cm^{-1} and 574 cm^{-1}, which are in good agreement with the previous reported results [20,21]. The weak peaks at around 415 cm^{-1} and 760 cm^{-1} should correspond to the second order Raman modes. With increasing x, the positions of Raman modes shift gently and some extra peaks due to structural phase transition are observed. As shown in the enlarged figure in Fig. 3(b), the Raman spectra of the x = 1.0 sample shows three additional peaks which further confirms its *Pccn* space group with lower symmetry. On the other hand, the Raman mode at around 204 cm^{-1} is assigned to the vibration of the Sr-O bond along c-axis in the A_{1g} configuration [22]. Previous studies on the relationship between structure and microwave dielectric properties of Ruddlesden-Popper structured materials have shown that the evolution of this mode has a close connection with the obtained Qf values [22,23]. With increasing x, an obvious

broadening of this mode is observed (see Fig. 3(c)), which might be closely related to the decay of microwave propagation.

The SEM micrographs of the present ceramics are shown in Fig. 4. The grain size and morphology vary significantly with compositions. For $x \leq 0.5$, the grains generally exhibit hexagonal shapes and the grain size decreases significantly at $x = 0.5$. With further increasing x, the grains turns to short columnar-like or/and plate-like morphology in $x = 0.75$. This may ascribe to the phase transition as discussed in the XRD results. The $x = 1.0$ sample demonstrates non-uniform microstructure with some abnormally long strip-like grains existed in the matrix, which might have an adverse effect on the microwave dielectric properties. Besides, it is worth noting that the morphology change leads to the less closely-stacked microstructure in the $x \geq 0.75$ samples, which could be another factor affecting the resulting microwave dielectric properties.

The variation of Qf value with composition x is shown in Fig. 5. With increasing x, the Qf value decreases monotonously from 145,000 GHz at $x = 0$ to 41,500 GHz at $x = 1.0$. The decline of Qf value should be discussed from both intrinsic factors and extrinsic factors, as the dielectric loss is notoriously dependent on various parameters such as porosity, phase composition, microstructure, etc [24]. In the present ceramics, the effects of secondary phase can be neglected owing to the absence of additional XRD peaks in the entire composition. Therefore, the decline of grain size at $x = 0.5$ and the following increase of porosity together with the abnormal grain growth at $x = 1.0$ should be the main extrinsic factors affecting the dielectric loss.

For the intrinsic part, the above-mentioned broadening of A_{1g} Raman mode at around 204 cm^{-1} correlates to the decreasing coherency of lattice vibration, and thus exhibits the deterioration of Qf value. Similar results about the inverse changing trend of Raman peak width and Qf value have also been reported in some other material systems [25-27]. On the other hand, packing fraction has been widely accepted as an effective parameter in correlating the structural evolution with Qf value [28, 29]. The packing fraction, defined by the sum of the volume of packed ions over the volume of a primitive unit cell, could be obtained from the following equation:

$$Packing\ fraction = \frac{volume\ of\ packed\ ions}{volume\ of\ unit\ cell} \times Z$$
$$= \frac{4\pi/3 \times [r_{Sr}^3 + (1-x)r_{Ti}^3 + xr_{Sn}^3 + 4 \times r_O^3]}{a \times b \times c} \times 4$$

where r_{Sr}, r_{Ti}, r_{Sn} and r_O are the effective ionic radii at each coordination number, a, b and c are the lattice parameters, and $Z = 4$ for the present ceramics with Ruddlesden-Popper structure. The calculated packing fractions of the present ceramics are plotted in Fig. 5. It is worth to note that the evolution of packing fraction demonstrates a similar changing trend with the Qf value, indicating that the decrease of packing fraction should be another major factor affecting the Qf value.

The variations of ε_r and τ_f of the present ceramics are shown in Fig. 6(a). ε_r decreases monotonously from 42 at $x = 0$ to 15.6 at $x = 1.0$. According to the Clausius-Mossotti equation, ε_r is mainly determined by the ionic polarizability per volume [30]. Therefore, the decrease of ε_r with increasing x could mainly attribute to the lower polarizability of Sn^{4+} (2.83 $Å^3$) than that of Ti^{4+} (2.93 $Å^3$) [31]. On the other hand, τ_f decreases with increasing x and the changing process could be divided into two stages. For $x < 0.75$, τ_f exhibits an approximately linear decrease with increasing x. With further increasing x, a rapid decrease of τ_f occurs until $x = 1.0$, from 39 ppm/°C at $x = 0.75$ to –155 ppm/°C at $x = 1.0$. Table 2 summarizes the microwave dielectric performances of the present ceramics and the optimal properties are obtained at $x = 0.8$ ($\varepsilon_r = 18$, $Qf =$ 70,500 GHz, $\tau_f = 2$ ppm/°C).

τ_f is closely related to the phase compositions, dielectric constant and structural phase transitions [2,30]. Because of the single phase nature shown in XRD patterns, the variation of τ_f should be mainly discussed from the dielectric constant and structural parameters. Fig. 6(b) plots the variation of τ_f value as a function of ε_r. An abrupt changing trend of τ_f value, characterized by a much larger slope, is observed at $x = 0.75$, exactly corresponding to the above-mentioned two phase zones. The figure inset gives the schematic illustration of the crystal structure evolution in the present ceramics. It is reasonable to infer that the onset of octahedral tilting in the *Pccn* space group should be the major factor determining the rapid decline of τ_f value at $x > 0.75$.

Moreover, considering that perovskite structure can be considered as a special kind of Ruddlesden-Popper structure with n = ∞ [14], the empirical relationship between τ_ε and tolerance factor obtained in perovskites may be applied in the $Sr_{n+1}Ti_nO_{3n+1}$ (n = 1, 2) series as well. Therefore, the converted τ_ε data of the present ceramics are compared with the tolerance factor curves of Reaney et al., for Sr and Ba based complex perovskites and $(Sr_{1-x}Ca_x)_3Ti_2O_7$ series (see Fig. 7) [12,14]. It is noteworthy that all the curves exhibit similar changing trends with tolerance factor. The τ_ε decreases approximate linearly with decreasing t in the composition range without octahedral tilting. While, the onset of octahedral tilting generally induces a rapid increase of τ_ε, which leads to the decrease of τ_f value ($\tau_f = -(\alpha_L + 1/2\tau_\varepsilon)$). On the other hand, the fitted τ_ε–t curves in $Sr_{n+1}Ti_nO_{3n+1}$ based ceramics could be applied in predicting the structure parameters of new temperature stable microwave dielectric ceramics and help invigorate the structure-performance tailoring mechanism of materials with Ruddlesden-Popper structure.

4. Conclusions

Single phase $Sr_2(Ti_{1-x}Sn_x)O_4$ (x = 0, 0.25, 0.50, 0.75, 0.80, 1.0) ceramics have been prepared via a standard solid state reaction method. The XRD patterns indicate a structure transformation from tetragonal to orthorhombic at $x \sim 0.75$, which is further confirmed using the Rietveld refinement and Raman spectra. The Qf value decreases approximate linearly with increasing x owing to the deteriorating microstructure and packing fraction. The τ_f-ε_r curve exhibits an abrupt decreasing trend due to the onset of octahedral tilting in the orthorhombic phase range. The optimum microwave dielectric properties are achieved at x = 0.80 (ε_r = 18, Qf = 70,500 GHz, τ_f = 2 ppm/°C). Moreover, it is also found that the tolerance factor has a close relationship with the crystal structure and microwave dielectric properties. This provides a new route to design the materials with required performance through adjusting the tolerance factor.

Acknowledgments

The present work was financially supported by Chinese National Basic Research Program under grant number 2015CB654601, National Natural Science Foundation of

China under grant number 51672063 and 51202051, Science and Technology Program of Zhejiang Province under grant number 2016C31110 and 2016C31006, Research Supporting Program of Hangzhou Dianzi University under grant number KYS045617113.

References

1. T. A. Vanderah, Talking ceramics, Science 298 (2002) 1182–1184.
2. I. M. Reaney, D. Iddles, Microwave dielectric ceramics for resonators and filters in mobile phone networks, J. Am. Ceram. Soc. 89 (2006) 2063–2072.
3. M. T. Sebastian, R. Ubic, H. Jantunen, Low-loss dielectric ceramic materials and their properties, Int. Mater. Rev. 60 (2015) 392–412.
4. X. M. Chen, Y. Xiao, X. Q. Liu, X. Hu, $SrLnAlO_4$ (Ln = Nd and Sm) microwave dielectric ceramics, J. Electroceram. 10 (2003) 111–115.
5. B. Liu, X. Q. Liu, X. M. Chen, $Sr_2LaAlTiO_7$: a new Ruddlesden–Popper compound with excellent microwave dielectric properties, J. Mater. Chem. C 4 (2016) 1720–1726.
6. L. Yi, X. Q. Liu, L. Li, X. M. Chen, $SrLn_2Al_2O_7$ (Ln = La, Nd, Sm) microwave dielectric ceramic new materials, Int. J. Appl. Ceram. Tec. 10 (2013) 177–185.
7. C. H. Lee, N. D. Orloff, T. Birol, et al., Exploiting dimensionality and defect mitigation to create tunable microwave dielectrics, Nature 502 (2013) 532–536.
8. B. Liu, L. Li, X. Q. Liu, X. M. Chen, $Sr_{n+1}Ti_nO_{3n+1}$ (n = 1, 2) microwave dielectric ceramics with medium dielectric constant and ultra-low dielectric loss, J. Am. Ceram. Soc. 100 (2017) 496–500.
9. T. Shimada, Far-infrared reflection and microwave properties of $Ba[(Mg_{1-x}Zn_x)_{1/3}Ta_{2/3}]O_3$ ceramics, J. Eur. Ceram. Soc. 24 (2004) 1799–1803.
10. S. Kawashima, M. Nishida, I. Ueda, H. Ouchi, $Ba(Zn_{1/3}Ta_{2/3})O_3$ ceramics with low dielectric loss at microwave frequencies, J. Am. Ceram. Soc. 66 (2010) 421–423.
11. E. L. Colla, I. M. Reaney, N. Setter, Effect of structural changes in complex perovskites on the temperature coefficient of the relative permittivity, J. Appl. Phys. 74 (1993) 3414–3425.
12. I. M. Reaney, E. L. Colla, N. Setter, Dielectric and structural characteristics of Ba-

and Sr-based complex perovskites as a function of tolerance factor, Jpn. J. Appl. Phys. 33 (1994) 3984–3990.

13. Y. Zhang, T. Shimada, T. Kitamura, J. Wang, Ferroelectricity in Ruddlesden-Popper chalcogenide perovskites for photovoltaic application: a role of tolerance factor, J. Phys. Chem. Lett. 8 (2017) 5834–5839.
14. P. L. Wise, I. M. Reaney, W. E. Lee, T. J. Price, D. M. Iddles, D. S. Cannell, Structure-microwave property relations in $(Sr_xCa_{(1-x)})_{n+1}Ti_nO_{3n+1}$, J. Eur. Ceram. Soc. 21 (2001) 1723–1726.
15. W. T. Fu, D. Visser, D. Ijdo, High-resolution neutron powder diffraction study on the structure of Sr_2SnO_4, J. Solid State Chem. 169 (2002) 208–213.
16. D. Kajfez, A. Gundavajhala, Measurement of material properties with a tunable resonant cavity, Electro. Lett. 29 (1993) 1936–1937.
17. B. W. Hakki, P. D. Coleman, A dielectric resonant method of measuring inductive capacitance in the millimeter range, IRE Trans. Microwave Theory Tech. 8 (1960) 402–410.
18. J. Zhang, R. Z. Zuo, Phase structural transition and microwave dielectric properties in isovalently substituted $La_{1-x}Ln_xTiNbO_6$ (Ln=Ce, Sm) ceramics, Ceram. Int. 43 (2017) 7065–7072.
19. B. Liu, L. Li, X. Q. Liu, X. M. Chen, Structural evolution of $SrLaAl_{1-x}(Zn_{0.5}Ti_{0.5})_xO_4$ ceramics and effects on their microwave dielectric properties, J. Mater. Chem. C 4 (2016) 4684–4691.
20. C. J. Fennie, K. M. Rabe, Structural and dielectric properties of Sr_2TiO_4 from first principles, Phys. Rev. B 68 (2003) 380–383.
21. S. Kamba, P. Samoukhina, F. Kadlec, et al., Composition dependence of the lattice vibrations in $Sr_{n+1}Ti_nO_{3n+1}$ Ruddlesden–Popper homologous series, J. Eur. Ceram. Soc. 23 (2003) 2639–2645.
22. M. M. Mao, X. Q. Liu, X. M. Chen, Structural evolution and its effects on dielectric loss in $Sr_{1+x}Sm_{1-x}Al_{1-x}Ti_xO_4$ microwave dielectric ceramics, J. Am. Ceram. Soc. 94 (2011) 2506–2511.
23. X. C. Fan, X. M. Chen, X. Q. Liu, Structural dependence of microwave dielectric properties of $SrRAlO_4$ (R = Sm, Nd, La) ceramics: crystal structure refinement and

infrared reflectivity study, Chem. Mater. 20 (2008) 4092–4098.

24. R. J. Cava, Dielectric materials for applications in microwave communications, J. Mater. Chem. 11 (2001) 54–62.
25. R. D. Shannon, Dielectric polarizabilities of ions in oxides and fluorides, J. Appl. Phys. 73 (1993) 348–366.
26. J. D. Breeze, J. M. Perkins, D. W. Mccomb, N. M. Alford, Do grain boundaries affect microwave dielectric loss in oxides? J. Am. Ceram. Soc. 92 (2009) 671–674.
27. M. Y. Chen, C. T. Chia, I. N. Lin, L. J. Lin, C. W. Ahn, S. Nahmd, Microwave properties of $Ba(Mg_{1/3}Ta_{2/3})O_3$, $Ba(Mg_{1/3}Nb_{2/3})O_3$ and $Ba(Co_{1/3}Nb_{2/3})O_3$ ceramics revealed by Raman scattering, J. Eur. Ceram. Soc. 26 (2006) 1965–1968.
28. A. Dias, V. S. T. Ciminelli, F. M. Matinaga, R. L. Moreira, Raman scattering and X-ray diffraction investigation on hydrothermal Barium Magnesium Niobate Ceramics, J. Eur. Ceram. Soc. 21 (2001) 2739–2744.
29. I. N. Lin, C. T. Chia, H. L. Liu, H. F. Cheng, R. Freer, M. Barwick, F. Azough, Intrinsic dielectric and spectroscopic behavior of perovskite $Ba(Ni_{1/3}Nb_{2/3})O_3$-$Ba(Zn_{1/3}Nb_{2/3})O_3$ microwave dielectric ceramics, J. Appl. Phys. 102 (2007) 044112.
30. E. S. Kim, B. S. Chun, R. Freer, R. J.Cernik, Effects of packing fraction and bond valence on microwave dielectric properties of $A^{2+}B^{6+}O_4$ (A^{2+}: Ca, Pb, Ba; B^{6+}: Mo, W) ceramics, J. Eur. Ceram. Soc. 30 (2010) 1731–1736.
31. M. Xiao, Q. Gu, Z. Zhou, P. Zhang, Study of the microwave dielectric properties of $(La_{1-x}Sm_x)NbO_4$ (x=0-0.10) ceramics via bond valence and packing fraction, J. Am. Ceram. Soc. 100 (2017) 3952–3960.
32. M. M. Mao, X. M. Chen, X. Q. Liu, Structure and microwave dielectric properties of solid solution in $SrLaAlO_4$-Sr_2TiO_4 system, J. Am. Ceram. Soc. 94 (2011) 3948–3952.

Table 1 Rietveld refinement results on powder XRD patterns of x = 0.75 and 1.0 ceramics at room temperature.

	x = 0.75	x = 1.0
Tetragonal phase	Space group: *I*4/*mmm*	
$a = b$ (Å)	4.00547(10)	–
c (Å)	12.62752(39)	–
V (Å^3)	202.593	–
Orthorhombic phase	Space group: *Pccn*	
a (Å)	5.67884(162)	5.73717(13)
b (Å)	5.69097(124)	5.72996(14)
c (Å)	12.57755(187)	12.58455(21)
V (Å^3)	406.483	413.701
R_p	7.86	8.52
R_{wp}	10.7	12.4
χ^2	6.16	6.93
Orthorhombic phase	34.42(1.26) wt%	100 wt%
Tetragonal phase	65.58(1.56) wt%	0 wt%

Table 2 The microwave dielectric properties of $Sr_2(Ti_{1-x}Sn_x)O_4$ (x = 0, 0.25, 0.50, 0.75, 0.80, 1.0) ceramics sintered at their optimal temperatures.

Composition	Sintering temperature	Microwave dielectric properties		
		ε_r	Qf (GHz)	τ_f (ppm/^{o}C)
x = 0	1500^{o}C/3h	42.0±0.8	145,000±1,800	130±8
x = 0.25	1575^{o}C/3h	32.9±0.6	115,700±1,300	107±6
x = 0.50	1650^{o}C/3h	24.7±0.5	95,000±820	86±4
x = 0.75	1675^{o}C/3h	18.5±0.5	75,750±540	39±2
x = 0.80	1675^{o}C/3h	18.0±0.3	70,500±590	2±2
x = 1.0	1700^{o}C/3h	15.6±0.2	41,500±150	-155±5

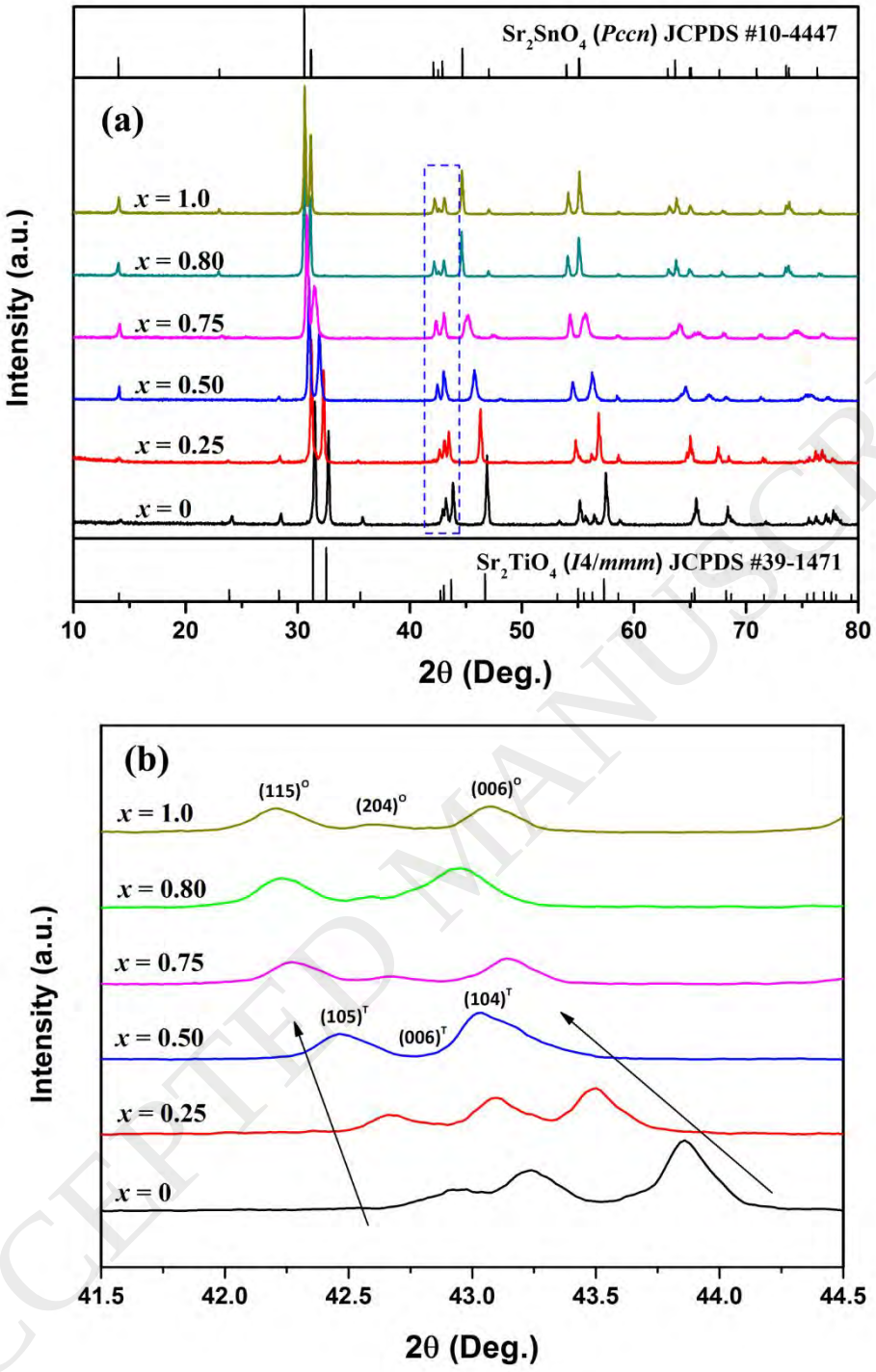

Fig. 1 (a) Powder X-ray diffraction patterns of $Sr_2(Ti_{1-x}Sn_x)O_4$ (x = 0, 0.25, 0.50, 0.75, 0.80, 1.0) ceramics. (b) Enlargement of the diffraction patterns in the 2θ range from 41.5° to 44.5°. The superscript letters (T and O) represent the crystallographic planes in tetragonal and orthorhombic phase, respectively.

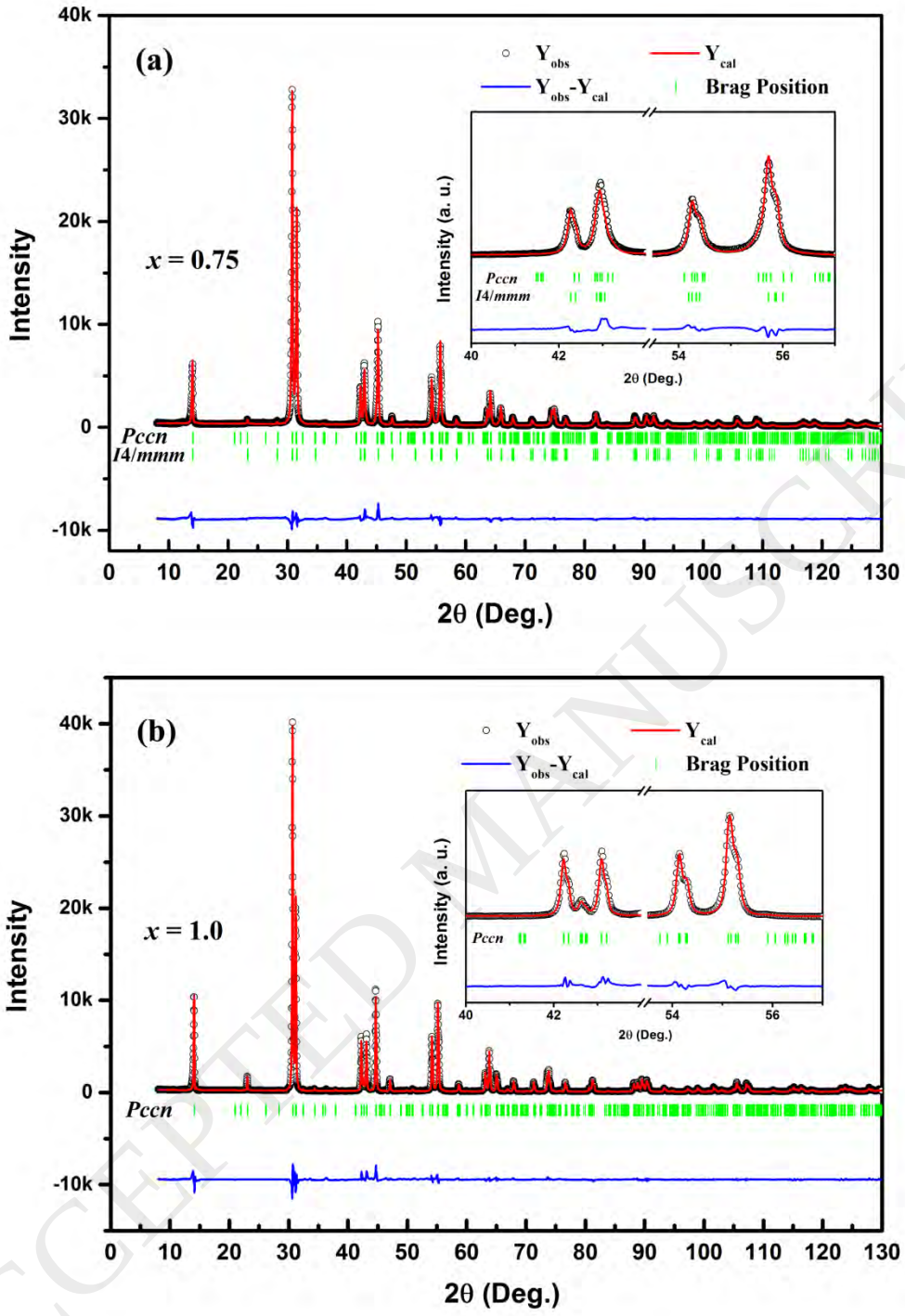

Fig. 2 Experimental (circles) and calculated (red line) XRD profiles for the (a) $x = 0.75$ and (b) $x = 1.0$ samples. The green short vertical lines below the patterns mark the positions of Bragg reflections. The bottom continuous line is the difference between the observed and the calculated intensity. The inset figures give the enlarged fitting results in the 2θ range from 40° to 57°.

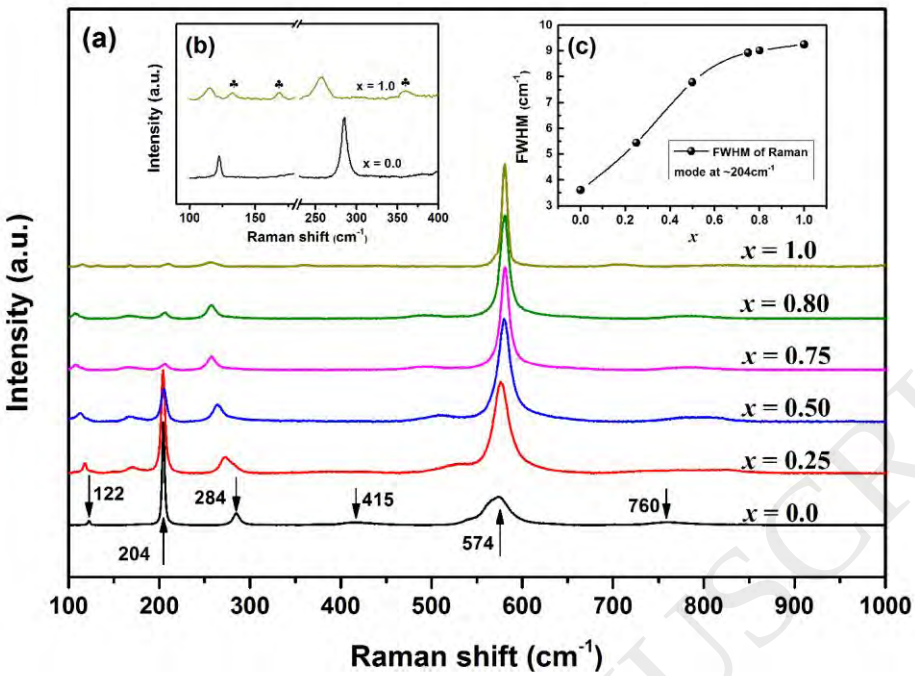

Fig. 3 (a) The Raman spectra of $Sr_2(Ti_{1-x}Sn_x)O_4$ (x = 0, 0.25, 0.50, 0.75, 0.80, 1.0) ceramics. (b) Partial enlargements of the Raman spectra of the x = 0.0 and x = 1.0 samples. (c) The FWHM (full width at half maximum) of the Raman mode at ~204cm^{-1} as a function of x.

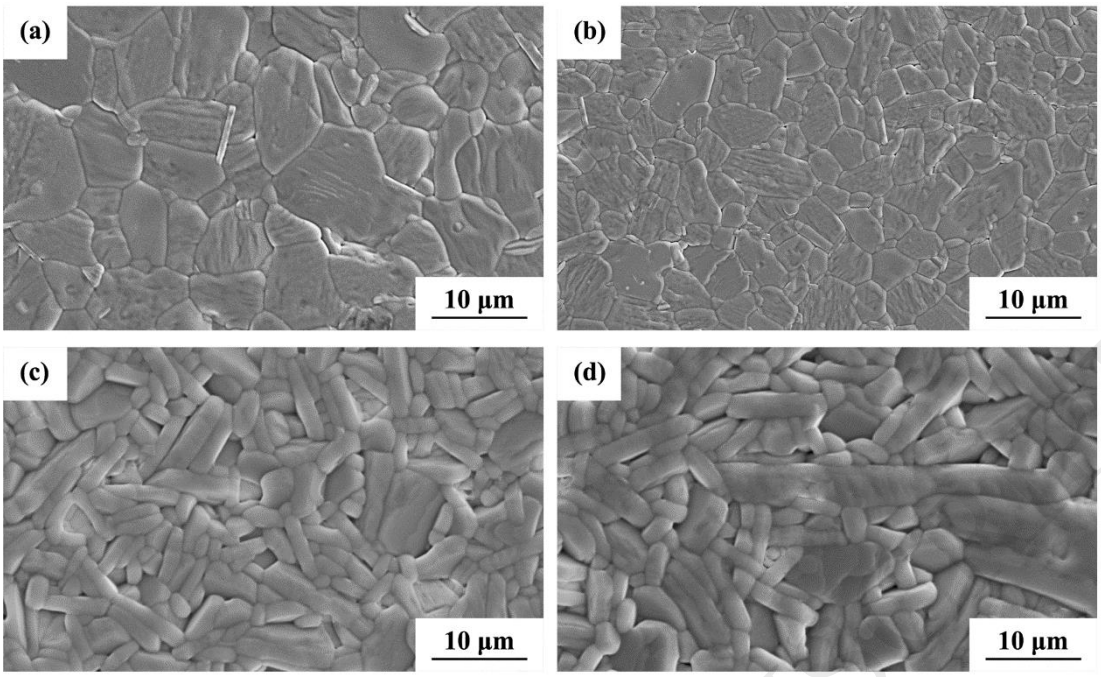

Fig. 4 SEM images of the polished and thermal-etched surfaces of $Sr_2(Ti_{1-x}Sn_x)O_4$ ceramics: (a) $x = 0$, (b) $x = 0.50$, (c) $x = 0.75$, (d) $x = 1.0$.

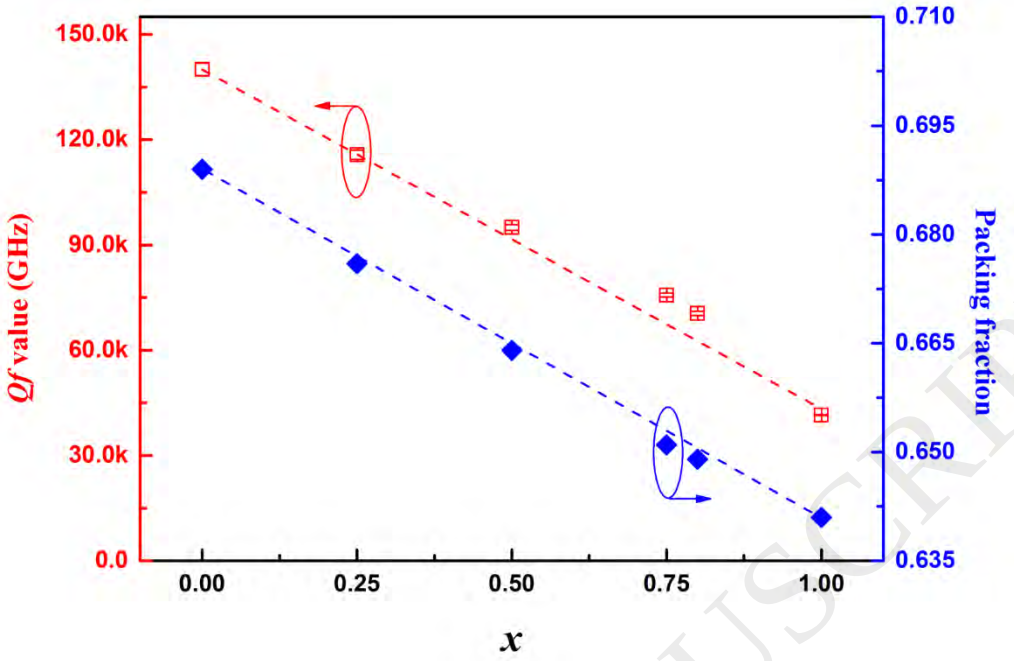

Fig. 5 The variation of *Qf* value and packing fraction of $Sr_2(Ti_{1-x}Sn_x)O_4$ ceramics with *x*.

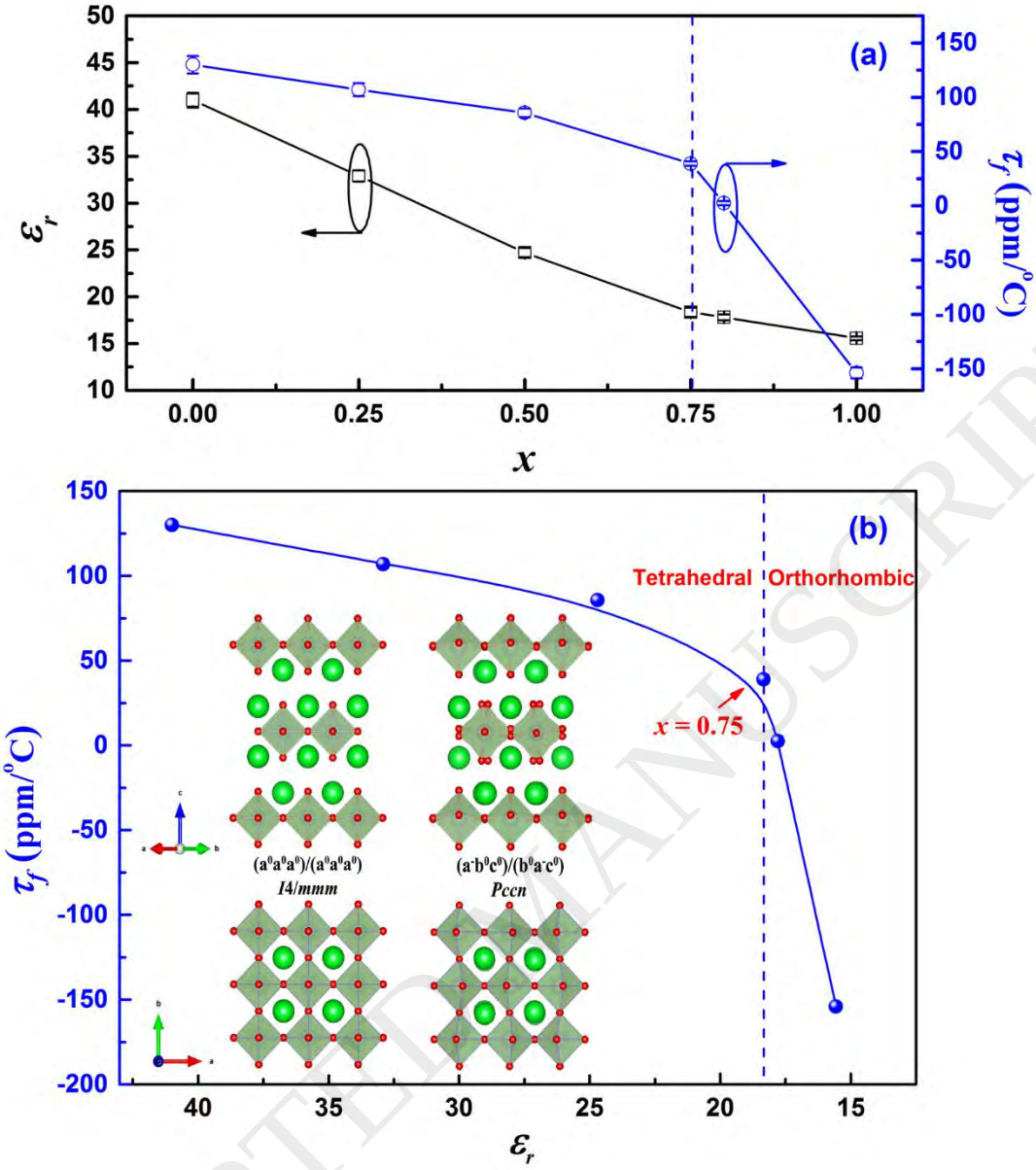

Fig. 6 (a) ε_r and τ_f of $Sr_2(Ti_{1-x}Sn_x)O_4$ ceramics as functions of x. (b) τ_f-ε_r relationship for $Sr_2(Ti_{1-x}Sn_x)O_4$ ceramics. The figure inset gives the crystal structures with *I*4/*mmm* and *Pccn* space group, respectively.

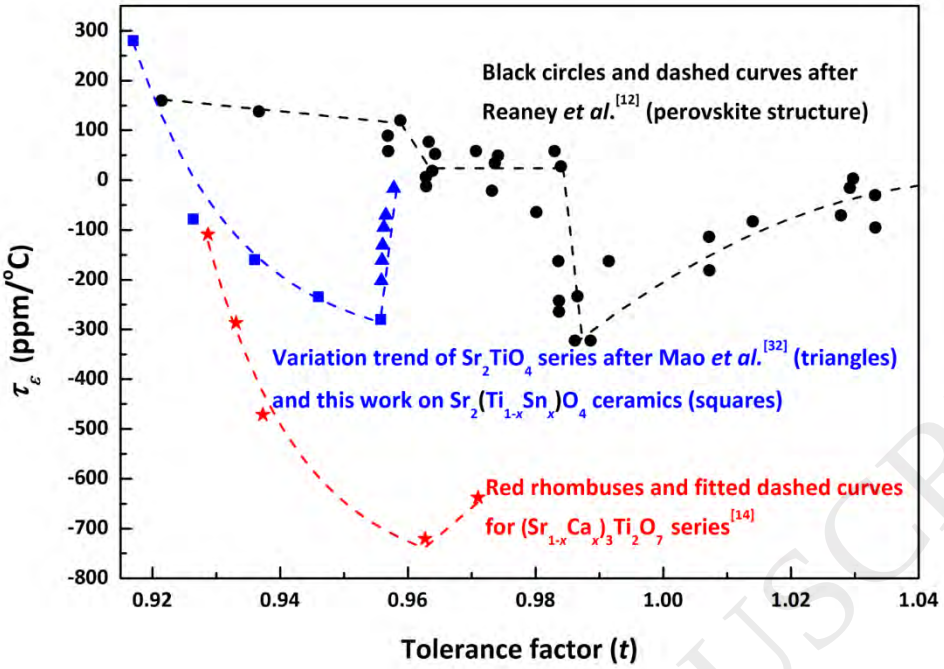

Fig. 7 Tolerance factor (t) verse τ_ε of complex perovskites and $Sr_{n+1}Ti_nO_{3n+1}$ based ceramics.